Colloids and Surfaces A: Physicochem. Eng. Aspects 448 (2014) 34–44

Contents lists available at ScienceDirect

Colloids and Surfaces A: Physicochemical and Engineering Aspects

journal homepage: www.elsevier.com/locate/colsurfa

Desiccation of a sessile drop of blood: Cracks, folds formation and delamination

B. Sobac[a,b,*], D. Brutin[b]

[a] Université Libre de Bruxelles, TIPs (Transfers, Interfaces and Processes), C.P. 165/67, av. F.D. Roosevelt 50, 1050 Brussels, Belgium
[b] Aix-Marseille Université, IUSTI UMR 7343 CNRS, 5 rue Enrico Fermi, 13013 Marseille, France

HIGHLIGHTS

- Influence of wettability on blood pattern formation.
- Good prediction of the initial crack spacing by the Allain and Limat model.
- Modelling of the evaporation rate evolution by a purely diffusive evaporation model.
- Cracks formation is followed by a delamination process and can be associated with folds formation.
- Numerous analogies with model suspensions.

GRAPHICAL ABSTRACT

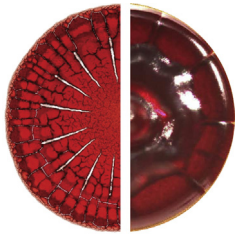

ARTICLE INFO

Article history:
Received 12 June 2013
Received in revised form 21 January 2014
Accepted 23 January 2014
Available online 12 February 2014

Keywords:
Drop
Evaporation
Cracks formation
Delamination
Colloidal suspension
Biological fluid

ABSTRACT

The drying of a deposited drop of blood leads to the formation of a complex pattern. Numerous coupled mechanisms are involved in this process, such as evaporation, flow motion, adhesion, gelation, crack formation and delamination. In this paper, we focus on the mechanisms related to the formation of cracks. The dynamics of fracture, the mean space cracking and delamination are examined. The initial crack spacing appears to be correctly predicted by the Allain and Limat model implemented for open geometries. The final pattern is highly dependent on the wettability of the substrate. Indeed, whereas a wetting situation leads to a ring-like deposit with regularly spaced radial cracks at the periphery and small-scaled disordered fractures at the centre, a non-wetting situation reveals a complex shape composed of radial cracks and folds due to the development of buckling instabilities. The different behaviours encountered were analysed with a stability diagram obtained for colloidal suspensions, and a good agreement was found. The study reveals numerous analogies between model suspensions and the fluid considered.

1. Introduction

The evaporation of sessile drops in the presence of solutes is an interesting phenomenon, allowing the formation of patterns. During the drying, the solvent evaporates and leads to a self-organisation of deposited particles on the surface, which leads to the formation of a final pattern. This system has received considerable attention from the scientific community during the past decade because of the many resulting applications, such as coating processes, ink-jet printing and spotting technologies for bio-assays.

* Corresponding author at: Université Libre de Bruxelles, TIPs (Transfers, Interfaces and Processes), C.P. 165/67, av. F.D. Roosevelt 50, 1050 Brussels, Belgium. Tel.: +32 2 650 29 45.
E-mail addresses: bsobac@ulb.ac.be, benjamin.sobac@gmail.com (B. Sobac), david.brutin@univ-amu.fr (D. Brutin).

http://dx.doi.org/10.1016/j.colsurfa.2014.01.076
0927-7757/

Since the work of Deegan et al. [1], the basics of the mechanisms that lead to the accumulation of solutes in a ring-like pattern along the contact line (called a "coffee stain") are well-known. These researchers noted that the evaporation rate is non-uniform and maximum in the vicinity of the contact line (for drops evaporating with small values of the contact angle, i.e., $\theta < 90^\circ$) in situations in which the drying is limited by the solvent diffusion. This situation leads to an outward flow inside the droplet that carries the solute to the self-pinned edge. Recently, other investigations completed the study of this flow in depth [2–4], and several studies were interested in understanding the fundamental mechanisms influencing the deposition phenomena, such as internal flow [5–7], the wettability [8,9] or the triple line dynamic [10,11] to find a means to control the final pattern.

During the drying process, when the solute concentration near the surface reaches a critical value, a skin is formed, which is generally considered as a gel [12]. A sol–gel transition (or solidification) occurs that is characterised by a change of the rheological behaviour with the appearance of a yield stress. In this situation, stresses develop inside the drying gel due to the competition between the evaporation of the solvent and the adhesion of the gel on the substrate [13,14]. If these stresses exceed the strength of the material, the formation is observed of cracks with various morphologies [15], ranging from craquelures to delamination or spiral patterns, leading to the formation of crack patterns. The concentration, the ionic strength, the presence of a surfactant, the thickness of the system and the deformability and the size of particles are among the parameters that influence this nonequilibrium pattern formation. The crack formation has been studied in various physical suspensions (polymeric and particle suspensions) and in various geometries (Hele-Shaw [16], sessile drop [17], capillary tube [18] or film [14]).

The drying of drops of biological fluids has been less widely studied, although it has been the subject of several investigations because of the potential applications in the field of medical diagnosis. Indeed, a number of studies were interested in linking diseases to the morphology of patterns resulting from the drying of a biological liquids [19]. The composition of biological fluids is altered by disease or diet and the deposited pattern resulting from the evaporation is altered by the composition of the liquid drop. Consequently, the final pattern could be used as a cheap and fast method of diagnosis of certain diseases [20]. However, only small number of studies were interested in explaining the physical or physicochemical mechanisms occurring during this process. Yet, a complex pattern composed by fractures results from such experiments most of the time. All of the studies dedicated to the understanding of the formation of these patterns have only focused on blood serum [21–23]. For instance, a regularly radial fracture structure is observed during the drying of bovine serum. A similar pattern has recently been observed with human blood [24,25] (Fig. 1). In the latter case, the flow induced by the solvent evaporation has been investigated. A capillary flow segregates and transports the solute to the edge, as in the coffee stain effect. The drying dynamics have also been examined, and a sol–gel transition has been highlighted. However, the process of crack formation in this system has never been studied. This article is dedicated to considering this point. The understanding of the pattern formation left from the drying of a drop of blood is of interest for forensic investigation [26] as well as for potential diagnosis of certain disease [27].

After a brief presentation of the experiments and blood properties in Section 2, a general description of the process is given in Section 3.1. The main mechanisms occurring in the problem and the different steps leading to the final deposit are introduced. A predictive model of the drying dynamic is then presented. Next, the mechanisms leading to the formations of cracks are approached in Section 3.2. The case fully discussed is focused on the crack pattern resulting in the desiccation of a drop in a hydrophilic situation. The dynamics of fracture and the mean crack spacing as a function of the deposit geometry are investigated, and a model predicting the initial mean space cracking is presented. We demonstrate that the cracks formation is followed by a delamination process. Finally, the study is extended to a non-wetting situation in Section 3.3. The final pattern is then clearly different: the final deposit is non-axisymmetric and includes folds. Analogies with physical suspensions are subsequently discussed.

2. Experimental

2.1. Set-up and experimental method

The experiments consisted of gently laying down a drop of blood with a syringe on a horizontal solid surface and observing the drops spontaneous evaporation into air. The evaporation occurs in a rectangular box measuring 100 mm × 100 mm × 150 mm (length × width × height) composed of transparent walls. The box protects the process from potential external flow perturbations. The box does not completely isolate the process from the outside because it is partially open on the upper surface. Next, the vapour concentration of the solvent at the infinity c_∞ is constant during the drying, and the ambient conditions (i.e., temperature T, pressure P, relative humidity H) inside the box are identical to the external ones recorded by a weather station (Lufft Opus).

A digital high-precision balance (Mettler Toledo XS 205) monitors the mass of the drop m during the drying with a resolution of 10 μg and an acquisition rate of 10 Hz. The evaporation rate dm/dt is directly derived from the mass evolution.

A digital camera (Canon EOS 7D) is positioned vertically in the experiment to provide a display in a top view. This device is fitted with a 1×–5× macro lens, which can obtain 5184 × 3456 pixels on an area of 22.3 mm × 14.9 mm. The resolution varies between 4.30 μm and 0.86 μm according to the choice of the enlargement. To improve the image quality and to avoid possible reflections of the surrounding light on the drop surface, a cold cathode back light at 5000 K ± 270 K (StockerYale ML-0405) was used as a unique source of light.

Another visualisation from the side was performed using a camera (JAI BM500GE, 15 images/s, 2456 × 2058 pixels) fitted with a microscope lens (VZM100i). This camera with a resolution of 4 μm could follow the geometrical parameters of the drop during the drying process. The captured images were processed with commercial software (Kruss DSA 30) to measure the contact angle θ, the height h and the wetting radius R of the drop at each time point.

Most of study presented considers a microscope glass plate as a substrate. The blood wets the glass with a contact angle of $\theta_0 = 15^\circ$. However, to observe the influence of the wettability on the process and the final pattern, a microscope glass plate coated by a nanolayer of gold is considered as the substrate in the last section. The blood subsequently wets the substrate with a contact angle $\theta_0 = 92^\circ$.

The blood considered for these experiments is human blood taken from healthy volunteers. The blood samples were taken in a medical laboratory. To perform numerous experiments at different times, the blood was stored in their original sterile tubes (BD Vacutainer 9NC 0.109 M) in a refrigerator at a temperature of +4 °C. These conditions preserve the blood. Experiments were performed within 6 days from donation to save blood from possible deterioration. The good reproducibility of the results shows that the storage conditions did not influence the drying dynamics. Before an experiment, the tubes were placed in a 3D orbital shaker at ambient temperature to homogenise the solution. This operation was performed for a long time such that the blood temperature reached the ambient temperature. The storage tubes have a KCl-coated layer on their walls for the neutralisation of the

Table 1
Distribution of formed elements of blood [28].

Formed elements	Typical quantity (units/mm^3)	Typical size (μm)	Volumic % of elements
Red blood cells	4.9×10^6	8	97
White blood cells	4.3×10^3	15	2
Platelets	2.4×10^5	3	1

fibrinogen, which is the protein responsible for the coagulation of blood when it is in contact with air.

2.2. Composition and properties of blood

Blood is composed of a liquid phase (plasma) in which formed elements are in suspension. The plasma is mainly composed of water and ions. Red blood cells, white blood cells and platelets compose the formed elements. This cellular matter, to which we will refer as particles, typically accounts for 45% of the blood volume and represents approximately 25% of the total mass [25]. The distribution of the formed elements of blood is reported in Table 1. According to the number of red blood cells and their volumetric distribution compared to the other formed elements, we simplify the system by considering blood as a two-phase liquid composed of water for the continuous phase and particles of 8 μm for the dispersive phase.

The physical properties of blood must be known to analyse the mechanisms developing during the drying process. The typical value of the blood density given in the literature [28] is $\rho_b = 1040\,\mathrm{kg\,m^{-3}}$. The rheological behaviour of blood was investigated using a rheometer (Anton Paar Physica MCR 501) for a range of shear rates from 1 to $100\,\mathrm{s^{-1}}$. A non-Newtonian relation between the shear stress τ and the shear rate $\dot{\gamma}$ was found, $\tau = k\dot{\gamma}^n$, where the power law n was found to be equal to 0.822 ± 0.001, and k is the consistency. Blood behaves most similar to a shear thinning fluid and its viscosity $\mu = \tau/\dot{\gamma}$ is approximately seven times higher than the viscosity of water. The surface tension was characterised using a pendant drop method. In terms of wettability, blood behaves similar to water because its surface tension $\gamma_b = 69.8\,\mathrm{mN/m} \pm 4.6\%$ is close to that of water ($\gamma = 72.0\,\mathrm{mN/m}$).

3. Results

3.1. General description

A drop of blood gently deposited on a microscope glass plate spreads quasi-instantaneously until reaching an initial wetting

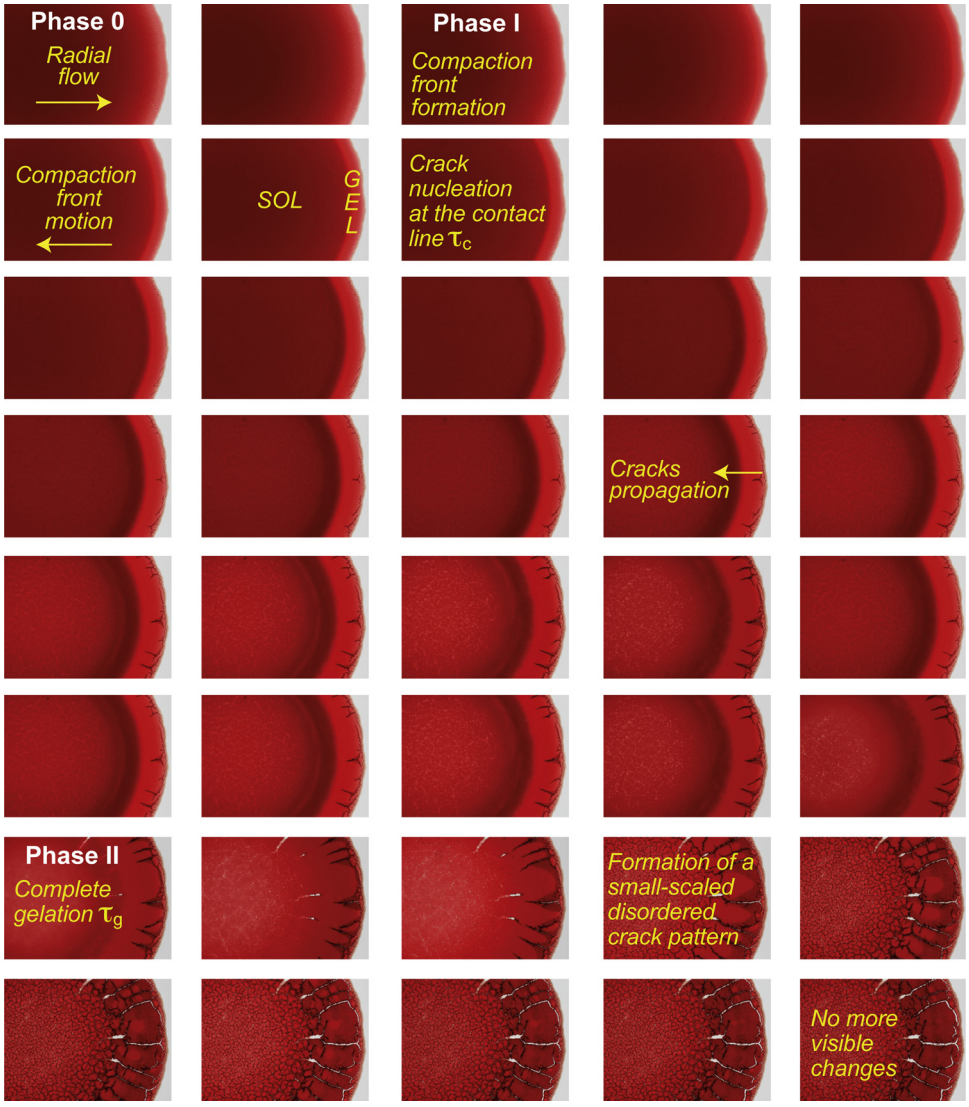

Fig. 1. Morphological evolution of a drying drop of blood (wetting radius: 3 mm). The duration between two consecutive pictures is 50 s.

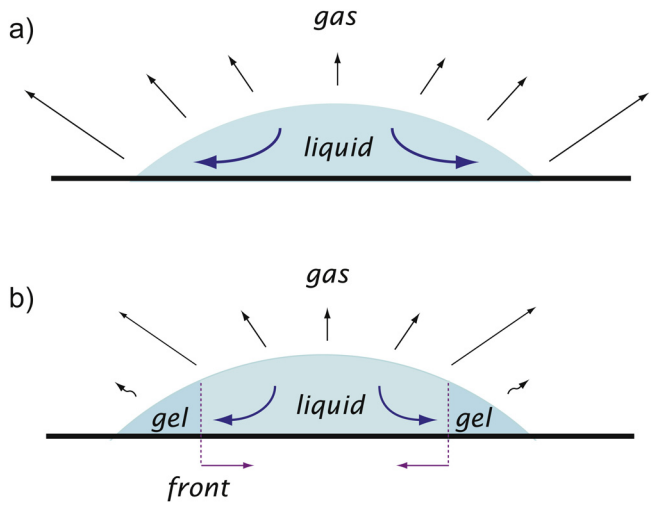

Fig. 2. Schematic view of the evaporation of a drop of blood in the pregelation phase (a) and in the gelation phase (b). During the gelation phase, the drop is composed of two regions: a fluid region, where particles are transported by the flow, and a gelled region, where particles are immobile.

radius and a contact angle of $\theta_0 = 15^\circ$. The blood thus shows a wetting behaviour on this surface. In contrast to a drop of water, which shrinks with an almost constant contact angle due to the low surface roughness of the glass, a drop of blood evaporates with a constant contact area, which is certainly due to the interactions between the non-volatile components and the substrate, which leads to an anchoring of the triple line [29]. This evaporation with a constant wetting radius over time is shown in Fig. 1. This sequence of pictures shows the morphological evolution of a drop of blood during drying from a top view. The process is composed of different stages:

- Phase 0: *Pregelation phase*. During the early time, the whole volume of the drop is liquid. During this stage, the solvent evaporates, and because the evaporation flux is more important close to the triple line in hydrophilic situations, a radial outflow develops [1,30,31]. The formed elements are then transported by this flow, and they accumulate near the contact line [24], reinforcing the contact line pinning. This mechanism is well known as the "coffee stain effect". At this time, the flow is dominated by capillary forces, and the formed elements are transported at a speed of approximately 8 $\mu m\, s^{-1}$ [24]. This transitory phase is short; thus, its observation is sometimes difficult.

- Phase 1: *Gelation phase*. The particles continue to be transported by this flow, leading to an increase of the concentration at the vicinity of the contact line. The increase of particles concentration is especially important because the fluid volume is locally low and because it decreases during the evaporation. When the concentration reaches a critical value ϕ_g, the particles aggregate and form a gel [2,12,32], i.e., a porous media filled with solute. Thus, a sol–gel transition occurs during evaporation [25]. This structural evolution is accompanied by an important change in the local rheological properties. Indeed, the viscosity slowly increases locally and will suddenly tend to infinity. Consequently, a gelled foot develops close to the edge while the central area is still liquid. The drop is then rapidly split into two regions with relatively different dynamics along the radial direction, as illustrated in the sketch (Fig. 2):

  - a region where particles are radially transported by the outward flow to the contact line because the concentration is less than the gelation concentration ϕ_g.

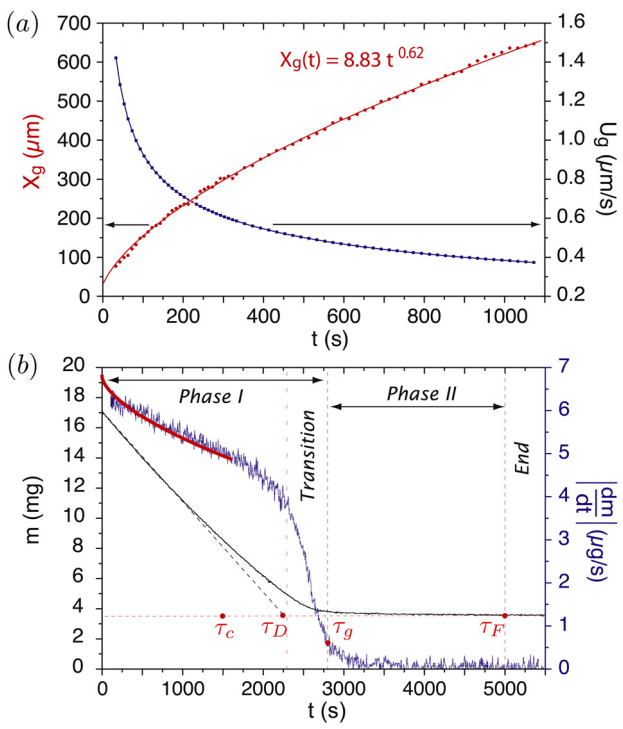

Fig. 3. (a) Evolutions of the position of the compaction front from the contact line x_g and of the front velocity U_g. (●) experimental data, (–) power law fits. (b) Evolutions of the mass m and the drying rate $|dm/dt|$. The dynamics reveals a sol–gel transition [25]. Phase I: Gelation Phase. Phase II: Postgelation phase. The experimental mass evolution is compared to the drying dynamic of a water drop in the same conditions (- -). The evaporation rate evolution is compared to the diffusion-controlled evaporation model by considering a drop drying with a receding triple line (–). (The initial and final masses and the wetting radius are, respectively, $m_0 = 17.3$ mg, $m_s = 3.51$ mg and $R = 4.3$ mm. Atmospheric conditions: $P = 1$ atm, $T = 22\,^\circ$C and $H = 42\%$.)

  - a region where the solute transport stops because the concentration is above the concentration ϕ_g.

A compaction front separates these two regions. This front radially propagates inward as a consequence of the outward flow. Behind the gelation front, a gelled region develops during evaporation at the expense of the liquid region. A track of the gelation front was performed, and the result is provided in Fig. 3a. The evolution of the position $x_g(t)$ and the velocity U_g of the front are plotted. The front was only tracked until 1100 s because it was not clearly perceptible after 1100 s. The dynamics of the compaction front are non-linear and monotone during the observed period. The position and the velocity of the front both have a power law dynamic. However, the front velocity is of the order of 1 $\mu m\, s^{-1}$. At a time τ_c, the first cracks nucleate on the gelled region at the vicinity of the contact line. Next, these cracks, which are regularly spaced radially, propagate inward as they are stretched by the front motion. Though the entire gelation phase occurs with a radial dynamic, the end of this phase is characterised by a fast and homogeneous gelation of the remaining fluid in the central area.

- Phase 2: *Postgelation phase*. At the time τ_g, the whole of the drop is gelled, and the drop is now solid-like. During gel formation, a part of the solvent is trapped inside the permeable porous matrix. Thus, the drying of the drop continues, and the cracks continue to develop. The radial cracks continue to propagate, and the development of a new pattern composed of small-scaled disordered fractures is observed at the centre.

3.1.1. Drying dynamics

The different phases also emerge in the drying dynamics. Fig. 3b presents the evolution of the drop mass m during the drying and the evaporation rate $|dm/dt|$. The mass evolution is non-linear and provides the mass of the non-volatile components of blood at the end of the drying process. The non-linearity of the mass evidences the presence of a mechanism that hinders the evaporation of the liquid phase, slowing the evaporation kinetics. Indeed, the mass evolution of a drying drop of pure water (water being the main component and solvent of blood) evaporating under similar conditions, i.e., with a constant wetting radius and a low value of the contact angle ($\theta_0 \approx 15^\circ \ll 40^\circ$), linearly decreases overtime (grey dotted line) [30,31,33]; the classical quasi-steady diffusion-controlled evaporation model predicting a constant evaporation rate, which is expressed as

$$\left|\frac{dm}{dt}\right| = 4D\Delta cR \quad (1)$$

where D is the diffusivity of the solvent vapour into air, $\Delta c = c_{sat} - c_\infty$ is the difference of the vapour concentration between the interface assumed at saturation and far from the drop $c_\infty \approx (1-H)c_{sat}$, H is the relative humidity and R is the wetting radius. Indeed, the evaporation process can be considered as quasi-steady since the ratio of the time of vapour diffusion into air to the drying time is low, $\tau_d/\tau_D \approx \Delta c/\rho \approx 2 \times 10^{-5}$. The desiccation time τ_D corresponds to the drying time of the drop only composed of the solvent of the solution. The decrease of the evaporation rate of the blood drop during evaporation is caused by the gelation of the drop. The formation of the permeable membrane leads to a decreased rate of evaporation. Indeed, the solvent now needs to move by permeation into the matrix to the gel/air interface to evaporate. Thus, the more the gelled region increases, the more the evaporation rate decreases. This drying dynamic is characteristic of the sol–gel transition [14,21]. The first phase corresponds to the *gelation phase* and has two sub-schemes. First, the evaporation rate slowly decreases before falling suddenly, which is related to the gelation dynamic. Gelation develops directionally with the radial propagation of the compaction front before occurring homogeneously at the centre. The last sub-scheme is then a transition to the complete gelation of the drop. The gelation time τ_g is defined as the time when the gelation is complete, i.e., the time at the end of the transition. The second phase corresponds to the *post-gelation phase*. The drop is solid-like but continues to dry because during the gelation, the compaction of formed elements traps the solvent. The time τ_F is the time of the complete drying of the drop. This value corresponds to the time when the evaporation is null and the drop mass is constant. The drying dynamics can give the values of the mean evaporation rate in the two phases. In the first phase, an evaporation rate of 4.84 $\mu g\,s^{-1}$ is obtained, whereas, in the second, a rate of 0.11 $\mu g\,s^{-1}$ is observed. The evaporation rate is then 44 times lower in the second phase. Indeed, the evaporation is controlled by the vapour diffusion into air in the first phase, but it is limited by the solvent diffusion through the matrix in the second phase. The quantity of evaporated solvent at the gel–air interface is relatively small compared to the one at the liquid-air interface, and thus it is relevant in a first approximation to assume that all of the evaporation occurs at the surface of the liquid area in the first phase. The surface of the liquid–air interface decreasing during the drying, and the drying dynamics can be described by the model previously described (Eq. (1)) by considering the receding gelation front $R(t) = R_0 - x_g(t)$ for the radius, where R_0 is the constant wetting radius. Then, we observe in Fig. 3b a good agreement between the model (red line) and the experiment until the gelation front is able to be tracked. The drying dynamic behaves in this first phase as a drop evaporating with a receding triple line.

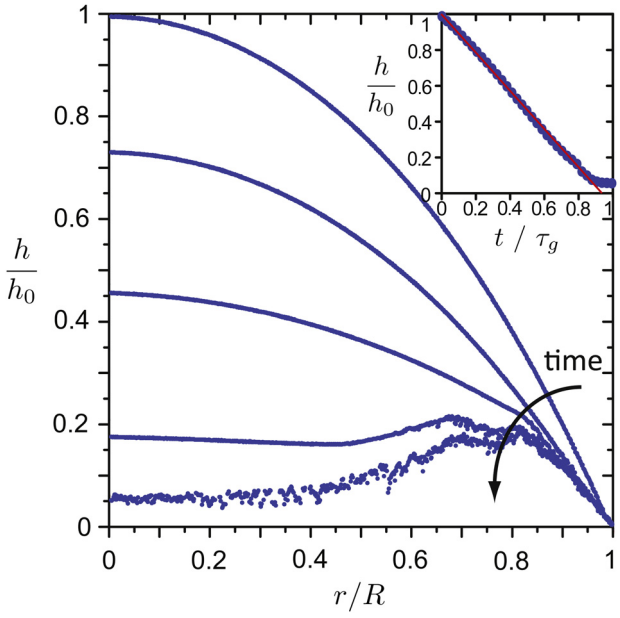

Fig. 4. Superposition of dimensionless profiles measured at different times by an optical confocal microscope (the duration between two consecutive profiles is 0.25 τ_g). Inset: time variation of the dimensionless apex height h/h_0.

3.1.2. Geometrical evolution and final deposit

Fig. 4a presents the dimensionless evolution of a drop profile during the drying. First, the drop evaporates similarly to a pure liquid, and the adopted profile is a spherical cap. Next, the appearance of a distortion of the interface at the vicinity of the contact line appears. This distortion is due to the inhomogeneity of the particle distribution resulting from the radial flow. The evolution of the profile then leads to the final shape of the deposit. The drop apex decreases linearly during almost all of the *gelation phase* (Fig. 4b). The profile evolution was measured with an optical confocal microscope. The geometry of the final deposit can be observed in Fig. 6b. This final deposit composed of the non-volatile components of the solution reveals an intermediate geometry between a pancake and a torus. This is a classical shape caused by the "coffee stain effect". The inhomogeneity of the particle distribution confirms the existence of a radial flow advecting the particles from the bulk to the edge. Indeed, if no radial flow were present, the deposit profile should have a maximum at the centre of the wetting area because the initial composition of the drop was homogeneous. In this case, the distribution is clearly non-homogeneous and presents a maximum at the vicinity of the triple line. At the end, the external corona ($r/R > 0.55$) composed of trapezoidal plaques leading to the formation of radial cracks represents 84% of the volume of the deposit, whereas the central part ($r/R < 0.55$) composed by small-scaled disordered fractures is only 16% of the volume of the deposit.

The general aspects of the description of the drying of a drop of blood that has been presented is very similar to previous observations performed for the drying of drops of colloidal suspensions [17] or blood serum [21–23,34]. This succession of mechanism always appears to lead to a final pattern composed of regularly spaced radial cracks at the periphery when $\tau_D \sim \tau_G$.

3.2. Crack pattern formation

The drying of a drop of blood is characterised by the evolution of the solution to a gel saturated with solvent. When the gel is formed, this new porous matrix formed by the aggregation of particles continues to dry due to the evaporation of the solvent. This effect results in a consolidation of the gel. The system is subsequently

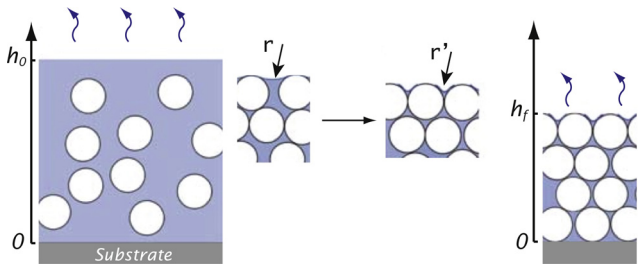

Fig. 5. Schematic representation of the formation of a porous matrix during the drying process [15]. A close packed array of particles saturated by solvent is formed. The system is bounded by two interfaces: the solid-gel interface and the gel–air interface. A curvature of the solvent–air menisci occurs at the evaporation surface and increases during solvent loss. The competition between the mechanisms occurring at the two interfaces, i.e., adhesion and evaporation, leads to crack formation.

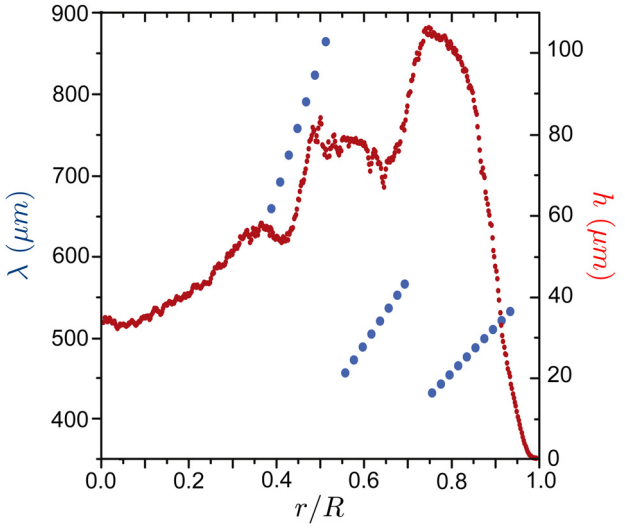

Fig. 6. Deposit thickness h and mean crack spacing λ as a function of the reduced position r/R. The data are related to the drop with a wetting radius of $R = 4.49$ mm in Fig. 7 and Table 2.

defined by two interfaces, as illustrated in Fig. 5: a gel–substrate interface, where the adhesion between the two media occurs, and a gel–air interface, where the solvent evaporates. At this latter interface, menisci form and are responsible for a capillary pressure $P_{cap} = -(2\gamma_{s,a}\cos\theta)/r_p$ in the liquid phase. $\gamma_{s,a}$ is the solvent–air surface tension, θ is the liquid–solid contact angle, and r_p is the pore radius. The curvature of the menisci increases with the evaporation, leading to a depression in the solvent filling the interstices. The effect of the pressure gradient ∇P leads to a migration of the solvent to the surface by Darcy's law [13]: $J = (\kappa/\mu)\nabla P$, where J is the flux of solvent through the matrix, which is equal to the evaporation flux of the solvent at the gel–air interface, μ is the dynamic viscosity of the solvent in the pore and κ is the network permeability of the gel. The pressure gradient also leads to a gradual shrinkage of the gel in response to the compressive force. However, the shrinkage of the matrix is limited by its adhesion to the substrate. The competition between evaporation and adhesion into the substrate leads to the development of tensile stresses that oppose the geometrical changes [35,36]. These mechanical stresses $\sigma \sim (\mu h J)/D$ increase during the drying and is relaxed through generation of cracks [16,17]. The failure of the media occurs when the elastic energy gained, by relaxing the material, balances the energetic cost of creating new area in the crack face [37]. During the drying of a drop of blood, a gelled foot forms at the contact line and propagates towards the centre of the drop. It leads to the development of orthoradial constraints in the consolidating gel leading to the formation of radial fractures [17,21]. The fracture propagation is correlated with the evolution of the field of mechanical stresses; the observed crack pattern strongly depends on physico-chemical interactions and the shape of the drop and of the deposit.

3.2.1. Initial cracking

The first cracks nucleate quite quickly after the beginning of the drying when $\tau_c = 0.25\tau_F$. These cracks nucleate at the edge of the drop, inside the gelled foot, whereas the drop centre is still fluid. Behind the receding gelation front, a regular pattern of radially spaced cracks appears in response to the development of orthoradial stresses. Following the global concentration of bio-particles during the drying of drops of blood, it was recently observed [25] that these cracks nucleate at a critical solid mass concentration of $\phi_s^c = 29.6 \pm 3.4\%$.

The unidimensional cracking of a colloidal suspension induced by evaporation was studied in a Hele-Shaw cell [16]. Allain and Limat found that the crack spacing λ is roughly proportional to the cell thickness e, and the authors proposed a simplified model that led to a relatively good prediction of their experimental data. Annarelli et al. [21] implemented this model for an open geometry, and a satisfactory agreement was also obtained with the initial crack spacing of drying drops of bovine serum albumin. To check the validity of this model on our system, scans of three drops of blood were performed with an interferometric microscope to accurately measure the initial average crack spacing λ_0^{exp} and the maximum height of the deposit h_{max}, which is also known as "foot height". The three drops have various initial masses to test the model for various initial crack spacings. Indeed, these lengths should vary with the height of the deposit [16,21,38], which increases with the drop size (see Table 2). The three drops can be observed in Fig. 7, and Table 2 provides additional information regarding these drops: the initial mass m_0, the wetting radius R, the foot height h_{max} and the initial average crack spacing λ_0^{exp}. The initial crack spacing appears indeed roughly proportional to the foot height.

Given the coupling between the gel elasticity and the diffusion of the solvent through the porous matrix, the model of Allain and Limat predicts that the dimensionless crack spacing $\Lambda = \lambda/e$ is a function of the dimensionless flux of solvent $K = (J_0 e)/(D_m C_\infty)$. This function can be approximated by $\Lambda = 0.522 - 0.716\log(K)$ for $K < 5 \times 10^{-2}$. J_0 is the flux of the solvent, D_m is the diffusion coefficient related to the transport of solvent in the porous medium, and C_∞ is the solvent volume fraction far away. To extend this model for open geometries and especially drops, Annarelli et al. considered that the same stress field exists in a drop foot as in one longitudinal half of the Hele-Shaw cell as a first approximation. This assumption means that the stress at the middle of the cell is null. The cell thickness is then equivalent to twice the foot height: $e = 2h_{max}$. The use of this model requires the knowledge of J_0, h_{max}, C_∞ and D_m. The foot height was accurately measured with an interferometric microscope. J_0 can be taken to be the same order as the mean volume rate of solvent loss $J_0 = V_s/(S_0\tau_D)$, where V_s and S_0 are, respectively the initial volume of the solvent and the free surface. $\tau_D \approx (\theta_0/4)((\rho R_0 S_0)/((dm/dt)_{t=0}))$, where τ_D is the desiccation time, R_0 is the wetting radius, θ_0 is the initial contact angle and ρ is the solvent density. The evaporation flux is approximately 10^{-7} m s^{-1}, but the exact values can be found in Table 2. The solvent volume fraction far away is approximately 55% (the volume fraction of solvent in blood). The difficulty of the prediction lies in the estimation of D_m, which is given by the product of the capillary characteristic velocity γ/μ and the hydraulic radius of the pore gel r, where γ and μ are the surface tension and the viscosity of the solvent (assumed to be water), respectively. Due to the difficulty in estimating the hydraulic radius of the pore, we considered the value previously used in the literature for colloidal suspension [16] and

Table 2
Data related to the three drops of blood presented in Fig. 7: the wetting radius, the initial drop mass, the foot height, the evaporated flux of the solvent, the experimental and theoretical values of the initial crack spacing and the relative deviation between the experimental data and the theoretical data.

R (mm)	m_0 (mg)	h_{max} (μm)	J_0 (m s^{-1})	λ_0^{exp} (μm)	λ_0^{th} (μm)	$\Delta\lambda$ (%)
2.74	5.2	68.59	1.29×10^{-7}	377	363	4
3.19	7.6	83.36	8.57×10^{-8}	432	465	8
4.49	19.0	104.48	5.41×10^{-8}	603	581	4

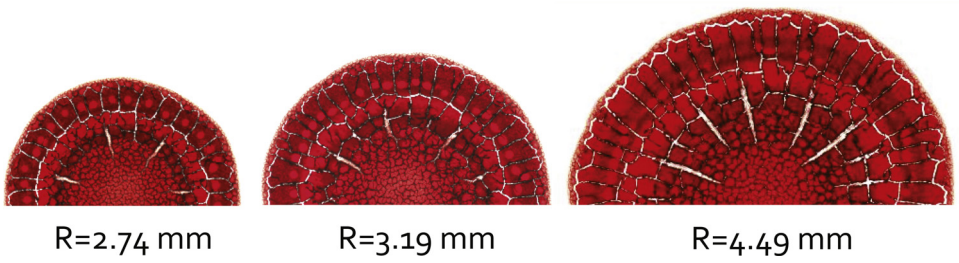

Fig. 7. Crack pattern as a function of the drop size. Complementary information for these drops are provided in Table 2.

bovine serum [21] for D_m, i.e., $D_m \approx 3 \times 10^8$ m^2 s^{-1}. Table 2 reports the initial crack spacing predicted by this model, λ_0^{th}, and their relative differences compared to the experimental values, $\Delta\lambda$. Despite the difficulty in estimating D_m and the degree of approximation of the model, there is a relatively good agreement between the model and the experiments because the relative deviation is $\Delta\lambda < 8\%$.

3.2.2. Cracking evolution

After the nucleation of cracks close to the edge, the cracks propagate radially towards the centre. The evolution of the mean crack spacing $\lambda = (2\pi r)/N_c$, which corresponds to the ratio of the perimeter where the cracks nucleate to the number of cracks crossing it, is shown in Fig. 6b. The crack formation is closely related to the geometry of the system, and the profile of the deposit is also reported in this figure. From the nucleation point, which is located at approximately 95% of the reduced radius, the mean crack spacing progressively decreases; and the number of cracks is constant. However, at two specific localisations, corresponding to local maxima, the number of cracks suddenly decreases. At these specific points, there is a sudden stop of the radial cracks, which join with a right angle the adjacent cracks. The presence of orthoradial stresses parallel to the edge lead to this mechanism. The cracks orthoradially merge with its neighbours, and consequently, a lower number of cracks continues to propagate towards the centre. Numerous studies on crack formation revealed that the crack spacing is roughly proportional to the thickness of the layer for various systems [16,38]. The results show that this relation is not always respected, as in our situation. The drying of a drop of bovine serum also revealed an unexpected variation of the crack spacing regarding the deposit profile [21]. The authors interpreted these results by assuming that crack propagation was not only purely induced by the gel drying but that the elastic behaviour of the material was also involved in the crack propagation. The radial cracks definitely stop at a reduced radius of approximately 45%.

At the centre of the drop, a small-scale, disordered pattern of cracks is observed. This central pattern is similar to the one formed during the drying of a colloidal suspension layer [15]. Indeed, as revealed by the evolution of the drop profile (Fig. 4a), the last moment of the drying of the central area is equivalent to the drying of a layer; the air–solution interface is relatively horizontal. The initial gelation occurs at the external corona of the drop with a gelation front radially propagating inward, but the gelation of the central area occurs quasi-homogeneously afterwards (Fig. 1). Thus, the directional growth of cracks is initially noticed; therefore, a successive generation of homogeneous cracks that invade the central region is observed in a second phase.

During the drying of a drop of blood, some of the mechanical stresses accumulated due to solvent evaporation are then released by the formation of cracks invading the gel. The system is then divided into numerous adjacent polygonal cells.

3.2.3. Delamination

The polygonal cells are still composed of a gel containing solvent, and the fluid contained in the interstices continues to evaporate from the upper surfaces. The thickness is then subjected to a strong stress gradient. As a result, the residual mechanical tensile stress gradually reincreases with time due to high capillary pressure. Each cell is then subjected to a compressive force on its drying face. When the stored elastic strain energy in the gel overcomes the adhesion energy of the gel attached to the substrate, the cells deform. Indeed, each polygonal cells buckles as its edges lift away out of the plane of adhesion, generating a concave shape [39] (Fig. 8). This process also allows a release of some of the stresses.

Because the substrate is transparent, the evolution of the adhesion between the drop and its substrate was observed using an inverted microscope (Leica DMI 3000 M) fitted with a digital camera (Canon EOS 7D). The adhesion is initially complete between the drop and its substrate, but after the cracking of the gel, a decrease of the adhering area between the newly created polygonal cells and the substrate is rapidly observed. This process preferably begins at the corners and edges of the cells due to the higher concentration of mechanical stresses in these locations [40]. A delamination front (i.e., the front which separates a detached region from the adhering one) develops and propagates from the edges to the centre of a cell. The mechanisms stop when the elastic strain is just balanced by the energy of adhesion [40]. At the final stage, each cells adheres in a localised area, as observed in Fig. 9. This figure presents the state of the two interfaces at the end of the drying. Areas of adhesion between the blood and the substrate are clearly distinguishable by their red colour while grey indicates a detachment of the gel (Fig. 9, bottom).

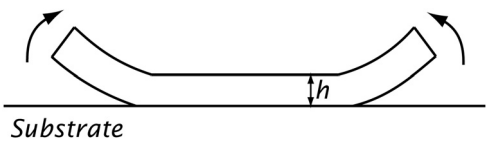

Fig. 8. Sketch of a single cell partially delaminated.

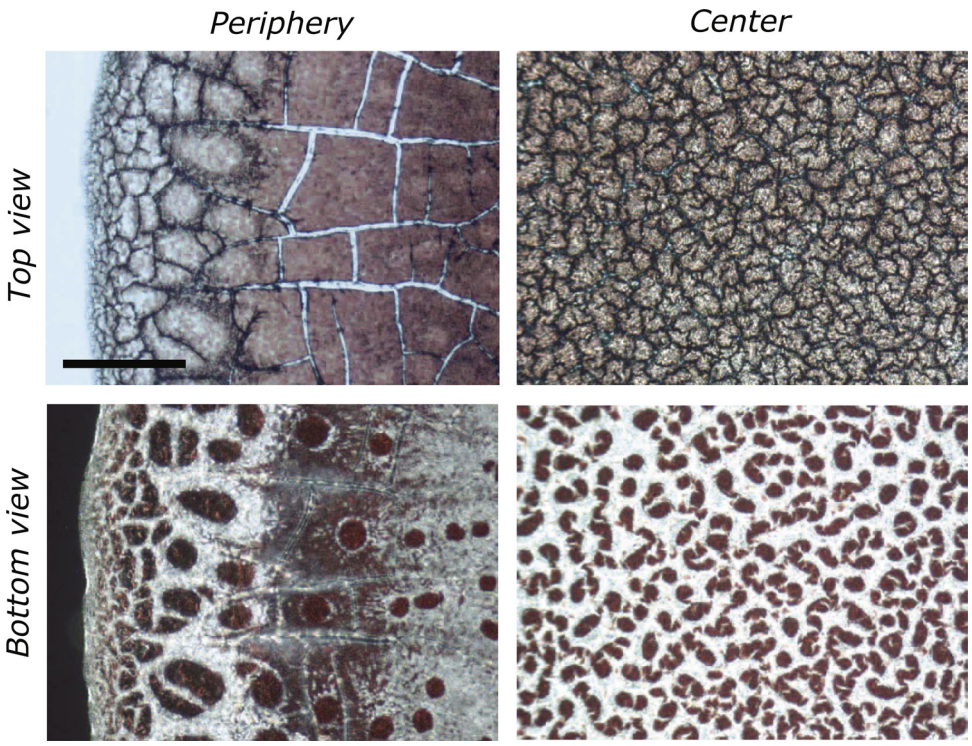

Fig. 9. Pictures of the crack pattern (top) and the adhering areas (bottom) at the end of the drying for various drop regions: external corona (left) and central area (right). The red areas denote the adhering areas. Scale: 0.1 mm. (For interpretation of the references to color in this figure legend, the reader is referred to the web version of the article.)

The ratio of the adhering area on the polygonal cell surface varies with the position in the drop. Indeed, prior studies revealed that the final adhering area notably depends on the gel thickness [15,40]. Thus, when the gel thickness is thin, i.e., for small polygonal cells (the central area of the drop), the buckling process is rapidly overcome by the adhesion of the layer on the substrate. As a result, the delamination process only occurs at the edges; the detachment area is accordingly small. In contrast, when the gel thickness is thick, i.e., for large polygonal cells (external corona of the drop), the adhering region shrinks more until the formation of a circular adhering region; the detachment area is thus more important. These observations are in total agreement with previous results concerning the desiccation of colloidal suspensions [14,15,40]. The experiments also revealed that the ratio between the adhering area and the cell area depends on the mass of the drop (the thickness of the deposit increasing with the mass as noted in Table 2) and the drying conditions (humidity). For all cases studied, a statistical study showed that the final adhering region represents between 30% and 50% of the initial adhering region in the central area of the drop. In the external corona of the drop composed by trapezoidal plaques delimited by radial cracks, this ratio decreases until it reaches between 0 and 10%. Indeed, when the layer thickness is sufficiently large, a complete de-adhesion was observed.

Delamination is a mechanism consecutive to the cracking of a gel. Consequently, for a drop, this process develops according to two dynamics. As the gelation and the crack formation initially propagate radially, the detachment of the gel begins at the edge of the drop and propagates towards the centre, as illustrated in Fig. 10. Thus, on the external corona, the delamination of what will be trapezoidal cells preferentially starts at the corners and, subsequently, the outermost edges and propagates inward following the crack formation. The delamination propagates first directionally. Afterwards, because the drying of the central area occurs as a colloidal suspension layer, delamination also occurs such as a layer, i.e., homogeneously over the entire polygonal cells forming this area. The partial detachment starts then from all polygonal edges.

3.3. Influence of the wettability

We previously observed that the drying of a drop of blood is a complex process where several mechanisms act, leading to the

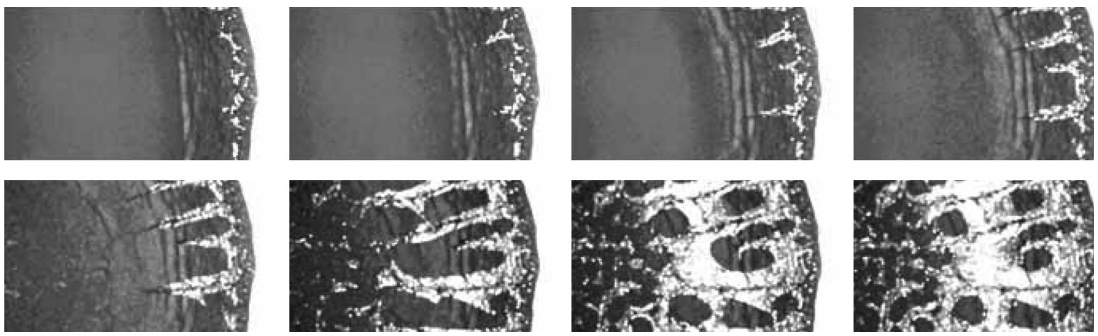

Fig. 10. Evolution of the adhesion of a drying drop of blood on a glass substrate. Bright areas correspond to the detached regions and dark areas correspond to the contact regions between the gel and the substrate.

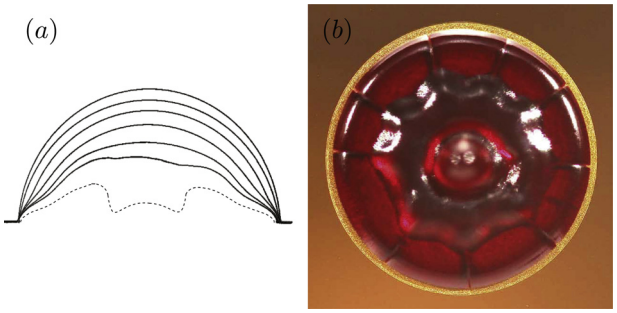

Fig. 11. (a) Evolution of the shape of a drop of blood drying with an initial contact angle $\theta_0 = 92^\circ$. Superposition of dimensionless profiles measured at different times by lateral imaging except the last one, which is a schematic view of the final deposit (the duration between two consecutive profiles is 360 s)[41]. (b) Top view picture of the shape of this drop at a time $t \approx 0.75\tau_F$.

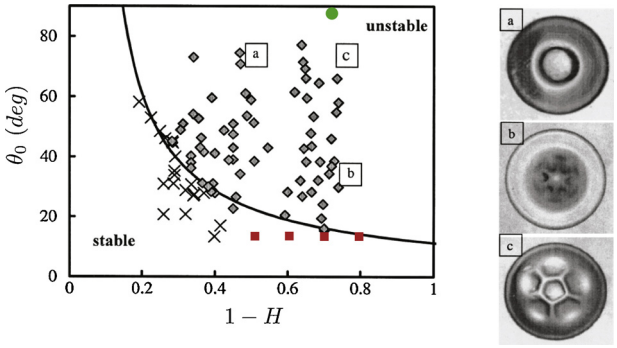

Fig. 13. Diagram of the various shapes displayed by the drying of a drop of Dextran ($\phi_m = 0.40$ g/g) following the initial contact angle θ_0 and the humidity rate $(1 - H)$ (result extracted from Pauchard and Allain [8]). The diagram is composed of two areas: a stable area, where the drying does not lead to the development of a buckling instability (×), and an unstable area, where the development of this instability causes the distortion of the surface and leads to complex shapes (♦). The various shapes revealed by the drying of a drop of blood ($\phi_m = 0.34$ g/g) are reported on the diagram: (■) glass substrate = stable evolution; (●) gold substrate = unstable evolution.

formation of a crack pattern: evaporation, hydrodynamics, gelation, cracking, and delamination. The previous pattern followed the evaporation of a drop of blood on a microscope glass plate, leading to the pattern formed during the drying in a hydrophilic situation with an initial contact angle of $\theta_0 = 15^\circ$. The deposit shape was then clearly a consequence of the coffee ring effect. What occurs with a higher value of the contact angle? What will be the shape of the deposit and the crack pattern? What is the influence of the contact angle on the development of these mechanisms? To investigate the influence of the contact angle on the drying of a drop of blood, we consider the drying of a drop on a glass plate coated with a nano-layer of gold. The substrate thus allows an initial contact angle $\theta_0 = 92^\circ$.

The example presented considers a drop with an initial mass of 9.5 mg drying in air at a temperature of 27 °C and a relative humidity of 25%. The final mass of the drop is 2.4 mg, and the mass concentration of the particles ϕ_m is 0.34 g/g. When a drop is drying with such values of the contact angle, the evolution of the drop profile is more complex than previously evidenced by Fig. 11a. First, the drop dries similar to a pure liquid drop with a spherical cap shape with a pinned contact line. Next, there is an axisymmetric deformation of the drop close to the triple line. Indeed, a foot builds. The curvature and the length of this foot increase with the decrease of the volume and the sinking of the drop. Finally, the distortion of the drop shape becomes more complex. A succession of elastic buckling instability develops, leading to the formation of radial folds and an inversion of the curvature at the top of the drop; this inverted region grows into a single invagination. The final morphology of the drop is no longer axisymmetric. Crack formation also occurs during the drying. In fact, cracks nucleate at the triple line and propagate with the formation of radial folds towards the centre of the drop. The number of radial cracks corresponds to the number of radial folds, as shown in Fig. 11b.

In this situation, there is a slight recession of the contact line during the drying, as indicated by the thin ring formed at the periphery of the drop in Fig. 11b. The drying of a drop of particle suspension leads to the formation of a gel [8,42] when the particle concentration reaches a critical concentration ϕ_g. The profile of the evaporative flux is homogeneous at the liquid-air interface [30] for an evaporating drop with a contact angle of 90°. The gas that escapes from this interface is driven outward by diffusion. The hydrodynamic instability of thermal Marangoni is negligible for water, and the solutal Marangoni is also initially negligible. The solution is homogeneous, and thus a radial flow develops from the bulk to the whole of the liquid–air interface. The particles are then transported by the flow to the free surface, where they pile up, leading to the formation of a shell of densely packed particles, as illustrated in Fig. 12. The shell undergoes a sol–gel transition; an elastic gelled skin forms at this interface. This envelope is sufficiently permeable to allow evaporation; thus, the solvent diffuses through the porous medium that forms the gel. During evaporation, the properties of the skin change due to the increase of its thickness. When the crust becomes sufficiently rigid, the drop volume continues to decrease while the free surface of the gel remains constant. The loss of the solvent trapped in the shell induces a depression inside the shell according to Darcy's law. Consequently, a stress gradient develops on the envelope thickness. A buckling of the shell results, which completely change the shape of the drop because the system prefers to concentrate these constraints in folds. The stresses continue to increase, and the drop weakens during drying. Thus, when the mechanical stress reaches a critical value, cracks nucleate at the contact line and propagate. At the end of the drying, the system consists of a fragile shell of complex morphology, as shown in Fig. 11b. The centre of the shell is only composed of air.

The same mechanisms have previously been observed during the drying of complex fluids such as polymer solutions or colloidal dispersions [8,42–45]. The final morphology of the drop is identical to the one obtained after the drying of a drop of Dextran [8] in similar conditions, as shown in Fig. 13c. This drop with a mass concentration of $\phi_m = 0.40$ g/g evaporated with an initial contact angle of 70° into air with a relative humidity of 30%. In their study on the drying of drops of complex liquids, Pauchard and Allain [8] studied the influence of wettability and humidity of the final shape of drops. Fig. 13 presents a stability diagram as a function of these two parameters with the various morphologies obtained. The mass concentration is notably close, and we therefore added the

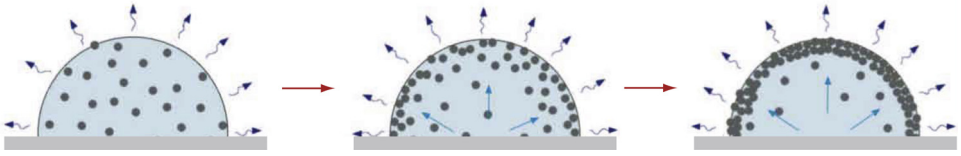

Fig. 12. Sketch illustrating the formation of a gelled crust caused by the accumulation of particles at the surface of a drop drying with an initial contact angle $\theta_0 = 90^\circ$.

various morphologies revealed by the drying of drops of blood to the diagram. The obtained results are in complete agreement with results reported regarding model suspensions. Indeed, the pattern observed after the drop drying on a glass substrate ($\theta_0 = 15^\circ$) does not show any buckling instability for any air humidity. However, when the evaporation kinetics is faster (weak humidity $H \approx 25\%$) and when the contact angle is important (for a glass substrate coated with a gold-layer, $\theta_0 \approx 90^\circ$), the drying reveals a complex shape consecutive to the development of elastic buckling instabilities.

Pauchard and Allain [8] determined an instability criterion in comparing the characteristic times of the problem. The desiccation time can also be expressed as

$$\tau_D = \frac{R_0^2 \beta(\theta_0)}{D c_{sat}(1-H)} \quad (2)$$

where R_0 is the initial base radius, θ_0 is the initial contact angle, D is the diffusion coefficient of the solvent into air, c_{sat} is the saturated vapour density, H is the relative humidity and $\beta(\theta) = ((1-\cos\theta)^2(2+\cos\theta))/((\sin^3\theta)(1.3+0.27\theta^2))$ when $0^\circ < \theta < 90^\circ$. This expression allows an estimation of the drying time of the solvent for our drop of blood deposited on the gold substrate of $\tau_D \approx 3100$ s. The prediction of the gelation time appears to be difficult. However, to simultaneously have a gelled area and a liquid area during drop evaporation, the gelation time τ_G has to be of the same order of magnitude as the desiccation time τ_D. Indeed, when the gelation time is higher than the desiccation time, i.e., $\tau_G/\tau_D \gg 1$, the drop is completely dried before the suspension has gelled. Conversely, when the desiccation time is higher than the gelation time, i.e., $\tau_G/\tau_D \ll 1$, the drop becomes gelled in its bulk before the end of drying. Thus, the drying is accompanied by a buckling of the gelled region, and the buckling time τ_B has to be lower than $\tau_D \sim \tau_G$. Indeed, for the drop of blood deposited on the gold substrate, the instability develops at $\tau_B \approx 2100$ s, which is before the desiccation time τ_D. In the case of an evaporating drop of blood on a glass substrate, any mechanical instability develops, which reveals that $\tau_B > \tau_D$.

4. Conclusions

The drying of drops of blood reveals the formation of complex patterns. The activator of the mechanisms leading to the deposit morphology is the evaporation of the solvent, which quasi-steadily diffuses in the atmosphere. The evaporative flux that develops at the drop interface provokes the development of an internal flow motion that transports the particles. When the concentration of particles reaches a critical value, they aggregate and form a reticulated media saturated in solvent, which is considered a gel. Due to the competition between the adhesion of the gel on the substrate and the solvent evaporation, the tensile stresses increase in the evaporating drop. Next, the formation of cracks and/or folds occurs according to the drying (humidity) and wetting conditions to release an excess of elastic stored energy.

The drying of a drop of blood has mainly been studied in hydrophilic situations. The experiments highlighted the radial propagation of the gelation front before the central area was homogeneously gelled as a layer of particle suspension. Due to the ortho-radial stresses, regularly spaced radial cracks directionally propagate at the vicinity of the contact line before a network of disordered small-scaled cracks appears in the central area. The solvent trapped inside the gel continues to evaporate, and a process of delamination of plaques occurs. The study notably revealed that the initial mean crack spacing is roughly proportional to the deposit thickness and is correctly predicted by the Allain and Limat model. Moreover, in the regime of directional propagation of the gelation front, we showed that the drying dynamics is equivalent to a drop of solvent evaporating with a receding triple line.

All of the mechanisms are linked, and the change of wettability highly affects the deposit shape. The evaporation of a drop of blood with an angle of 90° revealed the formation of a complex morphology due to the presence of an elastic buckling instability. In this situation, a shell forms during the drying and is deformed by buckling, leading to the formation of folds. The final shape is no longer axisymmetric.

The different behaviours encountered were assimilated to a stability diagram obtained for physical suspensions, and a good level of agreement was observed. The results presented are notably close to those obtained after the evaporation of drops of bovine serum, suspensions of colloidal particles and suspensions of polymers.

Acknowledgements

The authors would like to acknowledge N. Gueydon and J. Ettory for their assistance in preliminary experiments as well as F. Boyer, J. Colombani, B. Locquet and J. Sampol for fruitful discussions.

References

[1] R.D. Deegan, O. Bakajin, T.F. Dupont, G. Huber, S.R. Nagel, T.A. Witten, Capillary flow as the cause of ring stains from dried liquid drops, Nature 389 (1997) 827–829.
[2] H. Bodiguel, J. Leng, Imaging the drying of a colloidal suspension, Soft Matter 6 (2010) 5451–5460.
[3] Á.G. Marn, H. Gelderblom, D. Lohse, J.H. Snoeijer, Order-to-disorder transition in ring-shaped colloidal stains, Phys. Rev. Lett. 107 (2011) 085502.
[4] C. Monteux, F. Lequeux, Packing and sorting colloids at the contact line of a drying drop, Langmuir 27 (6) (2011) 2917–2922.
[5] V.X. Nguyen, K.J. Stebe, Patterning of small particles by a surfactant-enhanced marangoni-bénard instability, Phys. Rev. Lett. 88 (Apr 2002) 164501.
[6] W.D. Ristenpart, P.G. Kim, C. Domingues, J. Wan, H.A. Stone, Influence of substrate conductivity on circulation reversal in evaporating drops, Phys. Rev. Lett. 99 (Dec 2007) 234502.
[7] T. Kajiya, W. Kobayashi, T. Okuzono, M. Doi, Controlling the drying and film formation processes of polymer solution droplets with addition of small amount of surfactants, J. Phys. Chem. B 113 (47) (2009) 15460–15466.
[8] L. Pauchard, C. Allain, Stable and unstable surface evolution during the drying of a polymer solution drop, Phys. Rev. E 68 (Nov 2003) 052801.
[9] D.M. Kuncicky, O.D. Velev, Surface-guided templating of particle assemblies inside drying sessile droplets, Langmuir 24 (4) (2008) 1371–1380.
[10] J.R. Moffat, K. Sefiane, M.E.R. Shanahan, Effect of tio2 nanoparticles on contact line stick-slip behavior of volatile drops, J. Phys. Chem. B 113 (26) (2009) 8860–8866.
[11] H. Bodiguel, F. Doumenc, B. Guerrier, Stick-slip patterning at low capillary numbers for an evaporating colloidal suspension, Langmuir 26 (13) (2010) 10758–10763.
[12] T. Okuzono, K. Kobayashi, M. Doi, Final shape of a drying thin film, Phys. Rev. E 80 (2009) 021603.
[13] C.J. Brinker, G.W. Scherer, Sol–Gel Science: The Physics and Chemistry of Sol–Gel Processing, Academic Press, 1990.
[14] L. Pauchard, B. Abou, K. Sekimoto, Influence of mechanical properties of nanoparticles on macrocrack formation, Langmuir 25 (12) (2009) 6672–6677.
[15] V. Lazarus, L. Pauchard, From craquelures to spiral crack patterns: influence of layer thickness on the crack patterns induced by desiccation, Soft Matter 7 (2011) 2552–2559.
[16] C. Allain, L. Limat, Regular patterns of cracks formed by directional drying of a colloidal suspension, Phys. Rev. Lett. 74 (1995) 2981–2984.
[17] L. Pauchard, F. Parisse, C. Allain, Influence of salt content on crack patterns formed through colloidal suspension desiccation, Phys. Rev. E 59 (1999) 3737–3740.
[18] G. Gauthier, V. Lazarus, L. Pauchard, Alternating crack propagation during directional drying, Langmuir 23 (9) (2007) 4715–4718.
[19] V.N. Shabalin, S.N. Shatokhina, Morphology of Biological Fluids, Khrizopraz, Moscow, 2001.
[20] K. Sefiane, On the formation of regular patterns from drying droplets and their potential use for bio-medical applications, J. Bionic Eng. 7 (2010) 82–93.
[21] C.C. Annarelli, J. Fornazero, J. Bert, J. Colombani, Crack patterns in drying protein solution drops, Eur. Phys. J. E 5 (2001) 599–603.
[22] T. Yakhno, Salt-induced protein phase transitions in drying drops, J. Colloid Interface Sci. 318 (2) (2008) 225–230.
[23] Y.Y. Tarasevich, I.V. Vodolazskaya, O.P. Isakova, Desiccating colloidal sessile drop: dynamics of shape and concentration, Colloid. Polym. Sci. 289 (9) (2011) 1015–1023.

[24] D. Brutin, B. Sobac, B. Loquet, J. Sampol, Pattern formation in drying drops of blood, J. Fluid Mech. 667 (2011) 85–95.
[25] B. Sobac, D. Brutin, Structural and evaporative evolutions in desiccating sessile drops of blood, Phys. Rev. E 84 (2011) 011603.
[26] D. Attinger, C. Moore, A. Donaldson, A. Jafari, H.A. Stone, Fluid dynamics topics in bloodstain pattern analysis: comparative review and research opportunities, Forensic Sci. Int. 231 (2013) 375–396.
[27] K. Sefiane, Patterns from drying drops, Adv. Colloid Interface Sci. (2013), http://dx.doi.org/10.1016/j.cis.2013.05.002.
[28] M. Thieret, Biology and Mechanics of Blood Flows – Part II: Mechanics and Medical Aspects, Springer, New York, 2008.
[29] C.C. Annarelli, J. Fornazero, R. Cohen, J. Bert, J.-L. Besse, Colloidal protein solutions as a new standard sensor for adhesive wettability measurements, J. Colloid Interface Sci. 213 (1999) 386–394.
[30] H. Hu, R.G. Larson, Evaporation of a sessile droplet on a substrate, J. Phys. Chem. B 6 (106) (2002) 1334–1344.
[31] Y.O. Popov, Evaporative deposition patterns: spatial dimensions of the deposit, Phys. Rev. E 71 (2005) 036313.
[32] R. Zheng, A study of the evaporative deposition process: pipes and truncated transport dynamics, Eur. Phys. J. E 29 (2009) 205–218.
[33] B. Sobac, D. Brutin, Triple-line behavior and wettability controlled by nanocoated substrates: influence on sessile drop evaporation, Langmuir 27 (24) (2011) 14999–15007.
[34] Y.Y. Tarasevich, D.M. Pravoslavnova, Segregation in desiccated sessile drops of biological fluids, Eur. Phys. J. E 22 (2007) 311–314.
[35] F. Parisse, C. Allain, Shape changes of colloidal suspension droplets during drying, J. Phys. II France 6 (1996) 1111–1119.
[36] H. Lei, L.F. Francis, W.W. Gerberich, L.E. Scriven, Stress development in drying coatings after solidification, AIChE J. 48 (3) (2002) 437–451.
[37] M.S. Tirumkudulu, W.R. Russel, Cracking in drying latex films, Langmuir 21 (2006) 4938–4948.
[38] A. Groisman, E. Kaplan, An experimental study of cracking induced by desiccation, Europhys. Lett. 25 (1994) 415.
[39] Z. Neda, K.-T. Leung, L. Jozsa, M. Ravasz, Spiral cracks in drying precipitates, Phys. Rev. Lett. 88 (9) (2002) 095502.
[40] L. Pauchard, Patterns caused by buckle-driven delamination in desiccated colloidal gels, Europhys. Lett. 74 (2006) 188–194.
[41] D. Brutin, B. Sobac, C. Nicloux, Influence of substrate nature on the evaporation of a sessile drop of blood, J. Heat Transfer 134 (2012) 061101.
[42] N. Tsapis, E.R. Dufresne, S.S. Sinha, C.S. Riera, J.W. Hutchinson, L. Mahadevan, D.A. Weitz, Onset of buckling in drying droplets of colloidal suspensions, Phys. Rev. Lett. 94 (2005) 018302.
[43] L. Pauchard, Y. Couder, Invagination during the collapse of an inhomogeneous spheroidal shell, Europhys. Lett. 66 (5) (2004) 667–673.
[44] X. Chen, V. Boyko, J. Rieger, F. Reinhold, B. Reck, J. Perlich, R. Gehrkec, Y. Men, Buckling-induced structural transition during the drying of a polymeric latex droplet on a solid surface, Soft Matter 8 (2012) 12093.
[45] F. Boulogne, F. Giorgiutti-Dauphiné, L. Pauchard, The buckling and invagination process during consolidation of colloidal droplets, Soft Matter 9 (2013) 750.